PAPER

Cucurbit[7]uril-stabilized gold nanoparticles as catalysts of the nitro compound reduction reaction†

E. Blanco,*[a] I. Esteve-Adell,[b] P. Atienzar,[b] J. A. Casas,[c] P. Hernández[a] and C. Quintana[a]

The catalytic performance of cucurbit[7]uril-protected gold nanoparticles is reported for the first time for the reductive degradation of the banned but still used antibacterial compound nitrofurantoin. The cucurbit[7]uril-protected gold nanoparticles were produced by Au(III) reduction by sodium borohydride and subsequent addition of cucurbit[7]uril as a ligand. Working in this way, 5.7 nm gold nanoparticles were obtained and characterised by spectrophotometric and high-resolution transmission electron microscopic techniques. For a 1 : 100 nitro compound : sodium borohydride molar ratio, a normalised pseudo-first order apparent constant of 0.27 L s^{-1} m^{-2} at 25 °C and an activation energy of 34 kJ mol^{-1} were obtained. For comparative purposes, the reduction reaction of the pollutant 4-nitrophenol was also studied and an apparent kinetic constant of 0.12 L s^{-1} m^{-2} at 25 °C and an activation energy of 68 kJ mol^{-1} were obtained, data that, when compared with recently reported work, demonstrates that these nanoparticles are an efficient catalyst.

Introduction

The control of the nanoscale has permitted the development of new materials, structures, devices and systems such as nanotubes, nanowires, nanovalves and nanoparticles. Their applications extend to several areas as medicine, engineering, environment being the nanomaterials currently used in various fields such as electronics and cosmetics.[1–3] Gold nanoparticles (AuNPs) have attracted a significant interest due to their applications in catalysis, electronics or photonics. It is known that the size and shape of the nanoparticles play an important role on their properties, although the stabilizing agent employed to avoid their agglomeration can change their catalytic behaviour. Different protecting agents are usually employed (*i.e.*, citrate, thiols, surfactants or phosphorus-containing ligands)[4,5] and, more recently, the use of cucurbitnurils (CBns, $n = 5$–8, 10) has been proposed as a new stabilizing agent of metal nanoparticles.[6–10] This family of macrocyclic compounds is characterised by their pumpkin shape, hydrophobic cavity, rigidity with a 0.91 nm portal-to-portal distance and the carbonyl groups that delimit the entrance.[11–13] The oxygen atoms of these

groups are the responsible of the interaction with metal surfaces, initially discovered for flat gold surfaces,[14] later applied to stabilize metal nanosystems by means of several strategies.

The procedure described by Scherman *et al.* for the synthesis of CBn-protected metal nanoparticles is based on the use of borohydride as Au(III)-reducing agent and CB5–8 as stabilizing molecule of the previously formed (metastable) AuNPs.[6,7] Working in this way, long-term (up to 3 months) CB7-protected AuNPs of 7.5 nm diameter were produced. A different synthetic procedure was followed by Geckeler *et al.* who reported a series of works in which CB7 was also used as the reduction agent of gold, palladium and silver ions to produce metal nanoparticles in basic media.[8–10] The design of CB5-nanowires, the 1D-assembly of CB7 and AuNPs by means of electrokinetic techniques or the synthesis of ultraclean AuNPs followed by CB7 capping have been previously described.[15–17] In all these cases, the macrocycle acts as a glue between particles to generate assemblies with a clearly defined space between them, the above mentioned 0.91 nm, nanogaps ("hot spots") in the assemblies that involve high surface-enhanced Raman scattering (SERS) enhancement factors that could lead to single molecule detection.[18–21] Although CBn-stabilized metal nanosystems have been also applied for the construction of liquid crystal devices and immunoassays,[15,22] the catalytic performance on chemical reactions of CBn-covered metallic nanosystems have been scarcely investigated,[9,10] which is one of the aims of the work presented herein.

In this work, the catalytic performance of metal nanoparticles was tested in the best of our knowledge for the first

[a]Departamento de Química Analítica y Análisis Instrumental, Universidad Autónoma de Madrid. Cantoblanco, 28049 Madrid, Spain. E-mail: elias.blanco@uam.es; Fax: +34 91 4974931; Tel: +34 91 4974172

[b]Instituto Universitario de Tecnología Química CSIC-UPV, Departamento de Química, Universidad Politécnica de Valencia, 46022 Valencia, Spain

[c]Departamento de Química Física Aplicada, Universidad Autónoma de Madrid. Cantoblanco, 28049 Madrid, Spain

† Electronic supplementary information (ESI) available: Additional graphs and tables. See DOI: 10.1039/c6ra07168f

time to the reductive degradation of the antibacterial nitro-furantoin (NF), which is a broad-spectrum antimicrobial compound used in humans and animals and a member of the nitrofurans family. The EU and FDA banned the use of NF due to the toxicity, carcinogenic and mutagenic potency of the nitrofurans and their metabolites although they are still used in some countries.[23–26] The aquatic photochemistry of NF was investigated in environmentally relevant conditions[27] and in acid and basic aqueous medium subjected to thermal and photodegradation.[28] On the other hand, the action as catalyst of different biological reductases (i.e., cytochrome P450 reductase and nitro-reductases) in the reductive NF reaction by NAD(P)H has been investigated. In the case of mammals as rats and humans, the reduction by NADPH-cytochrome P450 reductase generates a nitro radical anion (which is oxidized by molecular oxygen) and hydrogen peroxide and the latter is responsible of the undesirable oxidative stress.[29,30] Bacterial nitro-reductases could reduce the nitro group to hydroxylamine or reduce the amide group to amine.[31] However, to the best of our knowledge the reductive cleavage of the antibiotic catalysed by metallic nanoparticles as reported in this work, has never been studied. Few reports about the electrochemical NF reduction can be found. Although these works are focused on the electroanalytical determination of the target compound, the discussion of the reduction mechanism is included.[25,26] However, the catalytic performance of metal nanosystems has been usually evaluated in the nitrophenols (4-nitrophenol, 4-NP) reduction reaction. So, to make a comparison with recently published works in which relatively good catalytic performances were reported, this reaction was also studied and the comparison with CB7-stabilized AuNPs is reported herein for the first time.

Experimental

Chemicals

Tetrachloroauric(III) acid trihydrate ($HAuCl_4 \cdot 3H_2O$) and $NaBH_4$ were obtained from Acros Organics (Geel, Belgium) and Riedel-de Haën (Seelze, Germany), respectively. Cucurbit[7]uril, 4-nitrophenol and nitrofurantoin were purchased from Sigma-Aldrich (St. Louis, Missouri, USA). Scharlau (Barcelona, Spain) provided ethanol and N,N-dimethylformamide. Ultrapure water was produced by an Ultra Clear™ TWF EDI UV of Siemens AG (Munich, Germany). 0.010 M stock solutions of 4-NP and NF were prepared in water and N,N-dimethylformamide, respectively.

Apparatus

HR-TEM images of the CB7-AuNPs were collected on a transmission electron microscope (JEOL JEM 2100F, Tokyo, Japan) under accelerating voltage of 200 kV. Samples were prepared by applying one drop of the as-synthesised gold nanoparticles in 50% (v/v) aqueous ethanol onto a carbon-coated copper TEM grid, and allowing it to dry at room temperature. TEM images were analysed by WSxM software (http://www.wsxmsolutions.com). The UV-Vis spectrophotometer used in this work was a UV-1800 of Shimadzu Corporation (Kyoto, Japan) equipped with a 10.0 mm quartz cuvette.

Synthesis of CB7-stabilized gold nanoparticles

CB7-protected AuNPs were synthesised as previously reported by Sherman et al. with slight modifications.[7] To this end, a 25 mL round-bottom flask was cleaned with aqua regia ($HCl : HNO_3$ 3 : 1 v/v; extremely corrosive, handle with care), rinsed several times with water and dried in an oven.[32] Next, synthesis solvent (10 mL, water : ethanol 1 : 1 v/v) was added followed by $HAuCl_4$ aqueous solution (34 μL, 0.030 M, 1.0×10^{-6} mol Au(III)) and the resulting solution was sonicated for 30 s. Then, under vigorous hand-swirling, a recently prepared $NaBH_4$ solution (25 μL, 0.1 M, 2.5×10^{-6} mol) in water was quickly added. The mixture was aged for 1 hour before the addition of a CB7 aqueous solution (0.5 mL, 2.0 mM, 1.0×10^{-6} mol) under vigorous swirling too. This colloidal gold suspension was aged for two days before any characterisation or use. All the preceding synthesis steps were conducted under ambient conditions.[7]

Catalytic reduction of nitro compounds

A freshly prepared $NaBH_4$ aqueous solution (0.2 mL, 0.050 M) was added to a 4-NP or NF aqueous solution (2.0 mL, 5.0×10^{-5} M) that was previously placed in a quartz cuvette. Next, a volume of the gold colloid suspension was added and the UV-Vis measurements were performed, in the 500–240 nm range, at regular intervals of time (30 s). When the influence of the catalyst concentration was studied, the volume of the synthesised colloidal gold suspension was varied (25 and 50 μL) and the volumes and concentrations of the contaminants solutions and of the reducing agent remained constant. When 25 μL of the colloidal gold suspension were used, the molar ratio Au : nitro compound : $NaBH_4$ was $1 : 41 : 4.1 \times 10^2$.

Study of the induction time

Firstly, in a set of experiments, the catalytic reaction was monitored by UV-Vis spectrophotometry when varying the order of mixing the reagents: (i) similarly as above, a 4-NP or NF aqueous solution (2.0 mL, 5.0×10^{-5} M) was mixed with a freshly prepared $NaBH_4$ aqueous solution (0.2 mL, 0.050 M) and 25 μL gold suspension was added to initiate the nitro compound degradation; (ii) a reactant (4-NP or NF) and gold nanoparticles were in contact for a fixed interaction time (20 minutes) before adding the $NaBH_4$; (iii) the gold suspension was added to a recently made $NaBH_4$ aqueous solution and, once 20 minutes passed, a 4-NP or NF aqueous solution was added. In all cases, the molar ratio Au : nitro compound : $NaBH_4$ was $1 : 41 : 4.1 \times 10^2$.

Secondly, UV-Vis spectrophotometry was employed to monitor the changes in the surface plasmon band of the gold suspension as a result of its interaction with reagents. In these experiments, gold suspension was mixed with 0.2 mL stock solution of nitro compound (0.010 M) or 0.2 mL freshly made $NaBH_4$ aqueous solution (1.0 M) to achieve the above molar ratios Au : nitro compound 1 : 41 and Au : $NaBH_4$ $1 : 4.1 \times 10^2$.

Results and discussion

Herein we present the results of an in-depth study of the catalytic performance of CB7-protected gold nanoparticles (AuNPs) in the reductive degradation of the banned but still used antibiotic nitrofurantoin (NF), process that has never been investigated in the presence of metal nanoparticles. The apparent kinetic constants and the activation energy of the catalysed reaction are presented. In addition, the 4-nitrophenol (4-NP) reduction reaction was investigated with the synthesised material as this reaction is frequently used to compare the catalytic performance of new synthetic procedures. The comparison with recently published works in which relatively good efficiencies were reported is included.

As it will be discussed below, the gold colloid synthesised by means of the procedure described in the Experimental section was stable and no precipitation was observed after three months at least. The nanoparticles were subjected to characterisation by high-resolution transmission electron microscopy and UV-Vis spectroscopy and were ready for the study of its catalytic performance after a two days ageing.

Nanoparticle characterisation by high-resolution transmission electron microscopy and UV-Vis spectroscopy

The synthesised AuNPs were characterised by High-Resolution Transmission Electron Microscopy (HR-TEM) and UV-Vis spectroscopy to obtain information related to its particle size, interparticle distance, crystallinity and concentration before to be used. Fig. 1(a) shows an example of the HR-TEM images obtained where quasi-spherical nanoparticles assembled in groups are observed. From the data of the histogram depicted in Fig. 1(b), a mean diameter of (5.7 ± 1.5) nm was calculated ($N = 100$). The mean nanoparticle diameter is lower than the

obtained by a similar methodology[7] that could be explained on the base of the glassware cleaning procedure followed. As reported previously[32] the use of aqua regia for cleaning all glassware material avoids unwanted AuNPs nucleation and aggregation. The lower mean diameter achieved by this modified procedure could be advantageous when the colloidal gold is subjected to catalytic studies as the surface-to-volume ratio is increased. The polydispersity (RSD of 26%) is in agreement with those reported when similar nanoparticles sizes were obtained (i.e. 23% and 25% for 7.5 and 3.6 nm nanoparticle diameters, respectively).[7,33]

Higher resolution images (Fig. 1(c)) allowed getting information about inter-particle distance and the crystallinity of the synthesised nanomaterial. As observed, the AuNPs of the group are separated by nano-gaps of 1.0 and 1.9 nm. More than 120 measurements of inter-particle distances were performed and the obtained results are resumed in the histogram depicted in Fig. 1(d). The Gaussian fits centred at 0.88 and 1.8 nm reveals that most of the inter-particle distances seem to be close to the above values and with similar frequencies. However, there is a minority group of AuNPs separated by longer distance at around 2.9 nm. As the crystallographic space between the CBn cavity portals is 0.91 nm, it is allowed to think that, in most cases, one or two CB7 could act as bridge of two adjacent nanoparticles. When triple of this number was found, three macrocycle molecules could separate the particles. When more than one CB7 is present, the simple union between adjacent macrocyclic molecules would led to repulsion between them due to the negative charge density of the cavity portals. The sodium ions present in the reaction flask, as a result of the use of sodium borohydride as reducing agent, could act as bridges to avoid this repulsion. These results are in accordance with those previously described.[7] Additionally, in the higher resolution image of Fig. 1(c), the lattice fringes revealing the nanoparticles crystallinity can be clearly observed. The interplanar distance between two consecutive planes was measured and it was found a value of 0.23 nm, which corresponds to the lattice spacing of Au(111) planes.[34–36] The gold crystallinity was corroborated by a Selected Area Electron Diffraction (SAED) pattern of a synthesised AuNP (Fig. S1(a), ESI†) and by a 2D-Fast Fourier Transform (2D-FFT) that was performed in the marked area of Fig. 1(c), which is shown in Fig. S1(b) (ESI†). The presence of the spots indicates the well-ordered arrange of gold planes. The crystallinity of the synthesised material is reported here for the first time.

The surface plasmon band (SPB) of the gold nanoparticle suspension prepared is localized at 530 nm (Fig. S2(a), ESI†) so the diameter of the synthesised AuNPs is in the 4–12 nm range.[32] The tabulated molar attenuation coefficient (at 450 nm) for AuNPs suspensions with a mean diameter of 6 nm, is $1.26 \times 10^{+7}$ M^{-1} cm^{-1}. If this value is assumed, a concentration of 2.1×10^{-8} M AuNPs is obtained.[32] On the other hand, and taking into account the 5.7 nm mean diameter obtained from TEM data, if a gold density of 19.32 g cm^{-3} is considered and if all Au(III) was reduced to Au(0),[17,37,38] a value of 1.03 m^2 L^{-1} was calculated for the total surface area S of the nanoparticles in the gold colloid suspension and an AuNPs concentration of
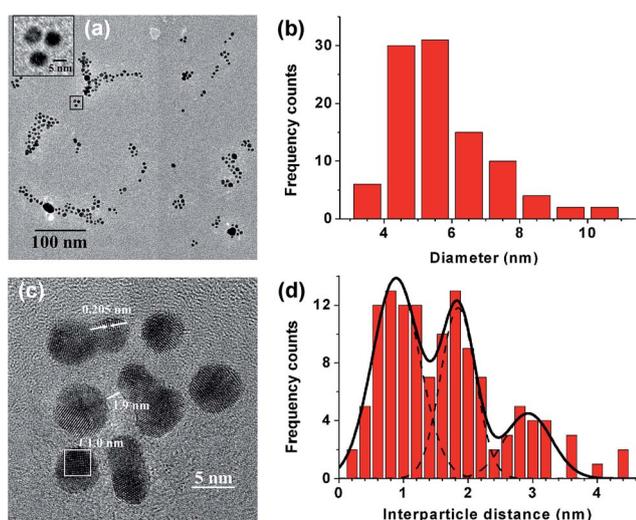
Fig. 1 HR-TEM images of AuNPs and results of their analysis. (a) Image of nanocrystal groups. The inset shows a magnification of the group marked. (b) Histogram of the nanoparticle diameter ($N = 100$). (c) Higher resolution image of a AuNPs assembly. (d) Histogram of the inter-particle distance ($N = 126$).

1.7×10^{-8} M was obtained, close to the 2.1×10^{-8} M AuNPs calculated from the UV-Vis measurement. X-ray photoelectron spectroscopy (XPS) spectrum analysis allows us to confirm that, in the experimental conditions, the Au(III) chemical reduction to Au(0) is complete (Fig. S3, ESI†).

As commented before, no precipitation was observed while working with the synthesised nanoparticles. In addition, as depicted in Fig. S2,† UV-Vis spectra recorded of the gold colloid during a period of 3 months ageing and the HR-TEM images obtained after this time did not show any significant change. These results reveal that the synthesised nanoparticles were stable for at least this period as reported previously.[7]

Catalytic performance of CB7-protected gold nanoparticles for the reduction reactions of 4-nitrophenol and nitrofurantoin

Two molecules were subjected to its catalysed degradation, namely nitrofurantoin (NF) and 4-nitrophenol (4-NP). The reductive degradation of the prohibited but still applied antibacterial NF is reported herein for the first time. The reduction of 4-NP was chosen because it is a model reaction usually employed to test new synthetic procedures of nanometric materials so the comparison between different catalyst can be made. Herein we present the results of an in-depth study of the catalytic performance of the synthesised nanomaterial in the NF and 4-NP reduction reaction. The apparent kinetic constants and the activation energies of the catalysed reactions are obtained and compared with recently published works in which relatively good performances were reported.

Once the characterisation of the synthesised gold colloid was performed that provided the mean nanoparticle diameter ((5.7 ± 1.5) nm) and the concentration (1.7×10^{-8} M AuNPs), features necessary for the thoroughly study of the CB7-stabilized gold suspension for its use as catalyst, systematic measurements were performed. In these, the catalyst amount was varied at a fixed temperature and, for a fixed volume of the gold colloid, the temperature was changed. These permitted to calculate the apparent kinetic constants and the activation energies, respectively.

Once the compound to be transformed, the reducing agent (sodium borohydride) and the catalyst were added to a cuvette, the reaction progress was followed by UV-Vis spectroscopy. The mathematical treatment of the signal was simplified considering that, when working with an excess of $NaBH_4$ respect of 4-NP such as herein, the data can be treated as a first-order kinetic with respect to the 4-NP concentration. In this conditions, the integrated rate equation is $\ln(C_t/C_0) = -k_{app}t$, where C_t is the 4-NP concentration at a time t, C_0 is the 4-NP initial concentration and k_{app} is the apparent pseudo-first order kinetic constant. As (C_t/C_0) is directly related to the ratio of the respective absorbances, therefore, k_{app} can be evaluated from the slope of the plot $\ln(Abs_t/Abs_0)$ *vs.* time.[3,33,37–42]

As detailed in the Experimental section, the compounds solutions were consecutively added for the 4-NP reduction reaction. A 5.0×10^{-5} M 4-NP aqueous solution is uncoloured but, upon addition of a $NaBH_4$ solution to obtain a $NaBH_4$/4-NP molar ratio of 100, the solution turns to an intense yellow that

reveals the presence of 4-nitrophenolate. This change in the solution was observed in the UV-Vis spectra in the form of a shift in the maximum of the absorption band from 317 nm (corresponding to 4-NP, black line in Fig. 2(a)) to 400 nm when 4-nitrophenolate is the predominant ion in solution as it is depicted in Fig. 2(a). Only when the AuNPs colloidal suspension was added, the reaction began so the 4-nitrophenolate band decreased and a new band at 315 nm (4-aminophenol, 4-AP, product of the reduction reaction) arose.

The experiment was carried out in the same way with a 5.0×10^{-5} M NF aqueous solution. The UV-Vis spectrum of the slightly yellow solution presented two absorption bands at 265 and 365 nm, as shown in Fig. 2(b) (black line). After the addition of the same excess of $NaBH_4$, a brighter yellow was developed and both bands presented a bathochromic effect showed by a shift to 280 and 390 nm, respectively. In this case, when the catalyst was added, the temporal evolution of the spectra is different to that observed with 4-NP. In the first step of the reaction, a decrease in the absorption at 390 nm was observed. After about 10 minutes of reaction, this main band split in three new bands at 345, 395 and 410 nm that could be assigned to different reaction intermediates that evolved a final product with absorption processes located at 260 and 345 nm. There are published reports of the NF electrochemical reduction mechanism involving the formation of several intermediates, processes in which the breakdown of the molecule takes place.[25,26] In order to obtain the k_{app} value for this nitro compound, the NF initial band located at 390 nm was monitored and, taking into account that $NaBH_4$ was in a 100 fold excess respect to NF, the above mathematical treatment of the signal *vs.* time was applied. Although the measurements were taken every 30 s, the graph of Fig. 2(b) shows the spectra obtained every 120 s for more clarity.

To evaluate the synthesised AuNPs catalytic activity in the reduction reaction of the target nitrocompounds, the influence of the concentration of the catalyst was studied and the results are depicted in Fig. S4 (ESI†). In both cases, the plots of $\ln(Abs_t/Abs_0)$ *vs.* time showed an elapsed time in which no variation of none of the nitro compounds concentrations was observed. This called "induction time" (t_0) results necessary to the diffusion and/or to the substrate-induced surface restructuring.[3,33,37–44] This induction time was subjected to investigation and the results are later exposed. Once this stage was reached,
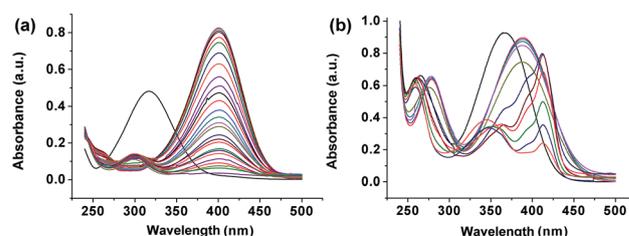

Fig. 2 Spectra of (a) 4-NP and (b) NF reduction catalysed by CB7-protected AuNPs. Black line: 5.0×10^{-5} M nitro compounds in water. Other lines are after the addition of $100\times$ $NaBH_4$ and a volume of the catalyst suspension, 30 µL for 4-NP and 25 for NF.

the signal varied noticeably in the case of NF, while 4-NP required higher AuNPs amount to observe this evolution. Finally, what is a common trend for both compounds is the fact that, without the catalyst, the reduction reaction did not progress. As stated above, the k_{app} values were evaluated from the slopes of the graph and the obtained results are summarized in Table 1. In this table, data of k_{app} normalised respect to the metal surface involved in the reaction and k_{app} normalised in terms of cost of the material (Au per nitro compound molar ratio) are also included. As expected, for both nitro compounds, higher catalyst amounts led to faster reduction reaction.[41,42] As shown by the k_{app} values obtained for all the catalyst volumes assayed during the study of NF reduction, the synthesised AuNPs show better efficiency as catalyst in this reduction reaction. These results were inferred from the comparison of the evolution in time of the UV-Vis spectra recorded during the assays (Fig. 2).

No experimental data supporting the corresponding inclusion complexes formation (CB7@4-NP and CB7@NF) have been obtained in the experimental reaction conditions assayed. On the other hand, the studied catalytic system can be compared in terms k_{app} values with previously reported catalytic systems in which other types of AuNPs stabilizing agents were used. To compare the catalyst efficiency of nanosystems in the 4-NP degradation, it should be considered that similar experimental conditions were employed. In other case, the comparison should be made in terms of normalised k_{app} values and the excess of NaBH$_4$ has also to be taken into account as it has influence on the apparent kinetic constant.[3,37,39,40] Considering all these points, a comparison of the results obtained with these CB7-stabilized AuNPs (25 μL colloidal gold suspension, 0.0116 m^2 L^{-1} area in the degradation reaction volume) with other metallic nanosystems, is presented in Table S1.† Apart from the good results recently reported by Deraedt et al.[33] (k_{app} of 0.36 L m^{-2} s^{-1}) that are explained on the base of the only use of NaBH$_4$ as stabilizing agent of AuNPs that could lead to an electrostatic stabilization of the AuNPs by BH$_4^-$/B(OH)$_4^-$ and Cl$^-$,[33] if the value of 0.12 L m^{-2} s^{-1} reported in this work is compared with other nanosystems as gold nanoparticles supported on silica nanotubes[34] or covalent organic frameworks,[36] better surface normalised k_{app} values are obtained. Different triazol ligands were compared with citrate or thiolate ligands to protect AuNPs and it was found that the citrate or thiolate-protected AuNPs were less efficient than the triazol-stabilized systems because triazoles formed softer bonds so they were easier displaced by the substrates of the 4-NP reduction reaction.[38] When the 6 nm AuNPs stabilized with these easily displaced ligands (1,2,3-

triazoles) were tested, a normalised apparent kinetic constant of 0.043 L m^{-2} s^{-1} was calculated.[38] Finally, if the comparison is made between the proposed nanoparticles and a similar nanosystem, made by palladium and stabilized by CB7,[10] more than a 10-fold increment in the apparent kinetic constant is obtained.

Induction time in the reduction reactions of 4-nitrophenol and nitrofurantoin

The induction time was frequently observed when the potential use of metallic nanoparticles as catalysts is evaluated and it is usually ascribed to diffusion and/or to the substrate-induced surface restructuring process.[3,33,37–44] However, there are cases in which this delay time was not found, for instance when the use of porous palladium nanoparticles allowed the establishment of a fast equilibrium between the reactants[43] or when gold nanoparticles were stabilized by sodium borohydride so the reducing agent was already present on the surface.[33]

In order to better understand the mechanism of the catalytic system, different experiments were carried out. On the one hand and according to Kalekar et al.,[44] a set of catalysed reactions was carried out in which the order of reactants addition was changed (see Experimental section). On the other hand, as the SPB depends on the size and shape of the metal nanoparticles and the surrounding medium,[2,4,38,45–47] we performed different experiments monitoring the shifts in the SPB respect to the time when the reactants were added.

The results obtained when the order of adding the reactants was changed (Table S2†) allow to us to think that sodium borohydride plays a relevant role in the induction time as, when the reducing agent was first mixed with the AuNPs, the lowest induction times were needed with respect to those required when any of the nitro compounds were first added (≈ 1.5 min for 4-NP and even, no delay time in the case of NF). However, and irrespective of the nitro compound, the longest induction times were achieved if borohydride was added the last (≈ 8.5 and ≈ 11 min for 4-NP and NF, respectively). In this case, borohydride ions should replace the nitro compound previously adsorbed on the nanoparticle surface. When both reactants should compete for the catalyst surface (AuNPs added the last), an intermediate situation was observed (≈ 6 and ≈ 7.5 min for 4-NP and NF, respectively). Similar results have been described by Kalekar et al.[44]

The results of all these experiments seem to support the surface reconstruction as described in the literature.[3,33,37–44] The catalytic reduction proceeds on the surface of the metal nanoparticles with an adsorption of the reactants: borohydride ions

Table 1 k_{app} values obtained for NF and 4-NP catalysed reduction reactions with different volumes of catalyst at 25 °C

Nitro compound	4-NP		NF	
V_{AuNP} (mol$_{Au(0)}$/mol$_{nitro}$, %)	25 μL (2.4)	50 μL (4.7)	25 μL (2.4)	50 μL (4.7)
k_{app} (s^{-1})	1.4×10^{-3}	3.5×10^{-3}	3.1×10^{-3}	7.8×10^{-3}
k_{app} (L m^{-2} s^{-1})	0.12	0.15	0.27	0.34
k_{app} (L (mol$_{Au(0)}$)$^{-1}$ s^{-1})	1.3×10^3	1.6×10^3	2.9×10^3	3.6×10^3

react with the surface of the nanoparticles to form a surface-hydrogen species to allow the reaction with the alongside 4-NP adsorbed on vacant sites of the gold nanoparticles.

The different behaviour exhibited by the nitro compounds would be ascribed to their differences in their adsorption process on the gold surface. As can be concluded from the second set of experiments carried out where SPB shifts produced by each reagent was monitored with the time (data not shown). The obtained results allow us to think that a faster adsorption of NF seems to be produced. In this case, the SPB of the AuNPs located at 530 nm shifts to ≈ 538 nm ($\Delta\lambda_{SPB} = 8$ nm) just when NF is added ($t = 0$) reaching a SPB shift up to 20 nm after 20 min. However, 4-NP adsorption influences in less extend leading to shifts in the SPB that range from 5 nm at $t = 0$ to 9 nm after 20 min.

Evaluation of activation energies for the reduction reactions of 4-nitrophenol and nitrofurantoin

In order to evaluate the apparent activation energy (E_a), the reduction of both compounds was monitored at different temperature values from 15 to 40 °C (25 μL of catalyst suspension). As expected, an increase in the temperature involved faster reactions with higher k_{app} values. Based on the Arrhenius equation $\ln k_{app} = \ln A - E_a/(RT)$, where A is the pre-exponential factor, E_a the apparent activation energy, R the universal gas constant, and T is the absolute temperature, E_a values of 68 and 34 kJ mol^{-1} were calculated for 4-NP and NF, respectively, from the slopes of corresponding plots of $\ln k_{app}$ *vs.* $1000/T$ (Fig. 3). From the results, it can be concluded that, either for the NF or 4-NP reduction, the catalytic behaviour of the synthesised AuNPs remains unaltered in the 15–40 °C range. The apparent E_a values obtained, higher than 20 kJ mol^{-1}, reveals that no limiting mass transport processes are governing the reactions. On the other hand, non E_a values are more close to that reported for "weak bonding" triazole ligands (25–40 kJ mol^{-1}) than to those reported for stronger bonding ligands as thiolates (132 kJ mol^{-1}).[38]

The results of kinetic constants and activation energies allow us to conclude that the synthesised CB7-protected AuNPs form relatively soft bonds to permit the substrate-induced surface restructuring but strong enough to avoid the colloid aggregation for the relatively long time of three months, at least. Moreover, the slightly higher apparent E_a values obtained for 4-NP system respect to that obtained for NF reaction, agrees with the higher induction times required for the 4-NP process as
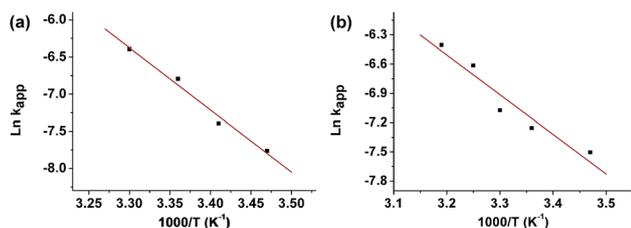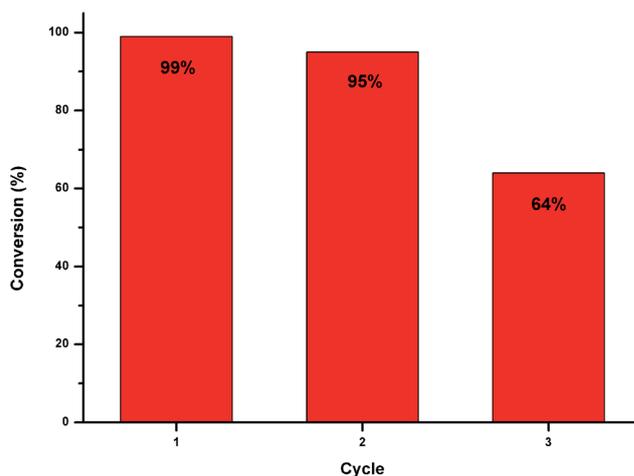

Fig. 4 Conversion percentages of 4-NP to 4-AP during consecutive cycles.

shown in the previously discussed assays (*i.e.* ≈ 3 min for 50 μL of AuNPs) unlike in the case of NF which no induction time is observed (see Fig. S4, ESI†).

Recyclability of CB7-protected gold nanoparticles

Finally, aimed for exploring the stability of the as-prepared catalyst, a recyclability study was performed. As can be observed in Fig. 4, these AuNPs respond satisfactory up to three cycles with conversion percentages evaluated to final 4-NP reduction reaction process higher than 60%. After the first cycle, no induction time was observed which is in good agreement with observations previously reported[48] and with the finding above mentioned supporting the catalyst mechanism proposed. When Au-based catalyst systems of higher particle size (*i.e.* 80 nm hollow porous AuNPs or 300 nm to 1 μm gold nanoflowers) recyclability data up to 5 or 6 cycles can be allowed.[49,50]

Conclusions

CB7-stabilized gold nanoparticles of (5.7 ± 1.5) nm diameter were synthesised and characterised by UV-Vis spectrophotometry and HR-TEM. High resolution microscopy images reveal AuNPs assemblies with relatively rigid separations between particles, probably due to the CB7 protection of the AuNPs, which acted as "glue" between the nanocrystals and being the majority joined by one or two macrocycles. The colloid was for the first time satisfactory applied to the catalysed reduction of the antibacterial nitrofurantoin. The high activity showed by the proposed catalyst for NF degradation could result in promising future applications of the nanosystems proposed. Moreover, the CB7-protected catalyst was also tested in the 4-nitrophenol reduction reaction for comparison with other nanosystems. The results in terms of normalised k_{app} and E_a obtained are comparable to other recently published works. Therefore, CB7 can be used as AuNP-stabilizing agent for an efficient reduction of the investigated nitro compounds.

Fig. 3 $\ln k_{app}$ *vs.* $1000/T$ plots for 4-NP (a) and NF (b). Volume of colloidal gold suspension of 25 μL.

Acknowledgements

Notes and references

1 C. Buzea, I. I. Pacheco and K. Robbie, *Biointerphases*, 2007, **2**, MR17–MR71.

2 C. Burda, X. Chen, R. Narayanan and M. A. El-Sayed, *Chem. Rev.*, 2005, **105**, 1025–1102.

3 P. Herves, M. Perez-Lorenzo, L. M. Liz-Marzan, J. Dzubiella, Y. Lu and M. Ballauff, *Chem. Soc. Rev.*, 2012, **41**, 5577–5587.

4 M.-C. Daniel and D. Astruc, *Chem. Rev.*, 2004, **104**, 293–346.

5 P. Zhao, N. Li and D. Astruc, *Coord. Chem. Rev.*, 2013, **257**, 638–665.

6 T.-C. Lee and O. A. Scherman, *Chem. Commun.*, 2010, **46**, 2438–2440.

7 T.-C. Lee and O. A. Scherman, *Chem.–Eur. J.*, 2012, **18**, 1628–1633.

8 T. Premkumar, Y. Lee and K. E. Geckeler, *Chem.–Eur. J.*, 2010, **16**, 11563–11566.

9 T. Premkumar and K. E. Geckeler, *Chem.–Asian J.*, 2010, **5**, 2468–2476.

10 T. Premkumar and K. E. Geckeler, *Mater. Chem. Phys.*, 2014, **148**, 772–777.

11 K. I. Assaf and W. M. Nau, *Chem. Soc. Rev.*, 2015, **44**, 394–418.

12 E. Masson, X. Ling, R. Joseph, L. Kyeremeh-Mensah and X. Lu, *RSC Adv.*, 2012, **2**, 1213–1247.

13 J. Lagona, P. Mukhopadhyay, S. Chakrabarti and L. Isaacs, *Angew. Chem., Int. Ed.*, 2005, **44**, 4844–4870.

14 Q. An, G. Li, C. Tao, Y. Li, Y. Wu and W. Zhang, *Chem. Commun.*, 2008, 1989–1991.

15 H. Sawai, T. Matsuura, H. Kakiuchi, T. Ohgi, Y. Shiraishi and N. Toshima, *Chem. Lett.*, 2012, **41**, 1160–1162.

16 N. Husken, R. W. Taylor, D. Zigah, J.-C. Taveau, O. Lambert, O. A. Scherman, J. J. Baumberg and A. Kuhn, *Nano Lett.*, 2013, **13**, 6016–6022.

17 A. Lanterna, E. Pino, A. Domenech-Carbo, M. Gonzalez-Bejar and J. Perez-Prieto, *Nanoscale*, 2014, **6**, 9550–9553.

18 S. Mahajan, T.-C. Lee, F. Biedermann, J. T. Hugall, J. J. Baumberg and O. A. Scherman, *Phys. Chem. Chem. Phys.*, 2010, **12**, 10429–10433.

19 C. Tao, Q. An, W. Zhu, H. Yang, W. Li, C. Lin, D. Xu and G. Li, *Chem. Commun.*, 2011, **47**, 9867–9869.

20 R. W. Taylor, T.-C. Lee, O. A. Scherman, R. Esteban, J. Aizpurua, F. M. Huang, J. J. Baumberg and S. Mahajan, *ACS Nano*, 2011, **5**, 3878–3887.

21 S. Kasera, F. Biedermann, J. J. Baumberg, O. A. Scherman and S. Mahajan, *Nano Lett.*, 2012, **12**, 5924–5928.

22 R. de la Rica and A. H. Velders, *Small*, 2011, **7**, 66–69.

23 P. Salgado-Figueroa, P. Jara-Ulloa, A. Alvarez-Lueje, L. J. Nunez-Vergara and J. A. Squella, *J. Electrochem. Soc.*, 2013, **160**, H553–H559.

24 N.-N. Du, M.-M. Chen, L.-Q. Sheng, S.-S. Chen, H.-J. Xu, Z.-D. Liu, C.-F. Song and R. Qiao, *J. Chromatogr. A*, 2014, **1327**, 90–96.

25 H. Channaa and P. Surmann, *Pharmazie*, 2009, **64**, 161–165.

26 C. Sridevi and S. J. Reddy, *Electroanalysis*, 1991, **3**, 435–438.

27 B. L. Edhlund, W. A. Arnold and K. McNeill, *Environ. Sci. Technol.*, 2006, **40**, 5422–5427.

28 A. Guzman, L. Agui, M. Pedrero, P. Yanez-Sedeno and J. M. Pingarron, *Electroanalysis*, 2004, **16**, 1763–1770.

29 P. Aracena, C. Lazo-Hernandez, A. Molina-Berrios, D. R. Sepulveda, C. Reinoso, J. I. Larrain, J. Navarro and M. E. Letelier, *Free Radical Res.*, 2014, **48**, 129–136.

30 Y. Wang, J. P. Gray, V. Mishin, D. E. Heck, D. L. Laskin and J. D. Laskin, *Free Radical Biol. Med.*, 2008, **44**, 1169–1179.

31 P. R. Race, A. L. Lovering, R. M. Green, A. Ossor, S. A. White, P. F. Searle, C. J. Wrighton and E. I. Hyde, *J. Biol. Chem.*, 2005, **280**, 13256–13264.

32 W. Haiss, N. T. K. Thanh, J. Aveyard and D. G. Fernig, *Anal. Chem.*, 2007, **79**, 4215–4221.

33 C. Deraedt, L. Salmon, S. Gatard, R. Ciganda, R. Hernandez, J. Ruiz and D. Astruc, *Chem. Commun.*, 2014, **50**, 14194–14196.

34 Z. Zhang, C. Shao, P. Zou, P. Zhang, M. Zhang, J. Mu, Z. Guo, X. Li, C. Wang and Y. Liu, *Chem. Commun.*, 2011, **47**, 3906–3908.

35 C. Zhu, L. Han, P. Hu and S. Dong, *Nanoscale*, 2012, **4**, 1641–1646.

36 P. Pachfule, S. Kandambeth, D. D. Dıaz and R. Banerjee, *Chem. Commun.*, 2014, **50**, 3169–3172.

37 S. Wunder, F. Polzer, Y. Lu, Y. Mei and M. Ballauff, *J. Phys. Chem. C*, 2010, **114**, 8814–8820.

38 R. Ciganda, N. Li, C. Deraedt, S. Gatard, P. Zhao, L. Salmon, R. Hernandez, J. Ruiz and D. Astruc, *Chem. Commun.*, 2014, **50**, 10126–10129.

39 S. Gu, S. Wunder, Y. Lu, M. Ballauff, R. Fenger, K. Rademann, B. Jaquet and A. Zaccone, *J. Phys. Chem. C*, 2014, **118**, 18618–18625.

40 S. Wunder, Y. Lu, M. Albrecht and M. Ballauff, *ACS Catal.*, 2011, **1**, 908–916.

41 S. Panigrahi, S. Basu, S. Praharaj, S. Pande, S. Jana, A. Pal, S. K. Ghosh and T. Pal, *J. Phys. Chem. C*, 2007, **111**, 4596–4605.

42 J. Zeng, Q. Zhang, J. Chen and Y. Xia, *Nano Lett.*, 2010, **10**, 30–35.

43 A. M. Kalekar, K. K. K. Sharma, M. N. Luwang and G. K. Sharma, *RSC Adv.*, 2016, **6**, 11911–11920.

44 A. M. Kalekar, K. K. K. Sharma, A. Lehoux, F. Audonnet, H. Remita, A. Saha and G. K. Sharma, *Langmuir*, 2013, **29**, 11431–11439.

45 M. Brust and C. J. Kiely, *Colloids Surf., A*, 2002, **202**, 175–186.

46 B. M. Reinhard, M. Siu, H. Agarwal, A. P. Alivisatos and J. Liphardt, *Nano Lett.*, 2005, **5**, 2246–2252.

47 C. Sonnichsen, B. M. Reinhard, J. Liphardt and A. P. Alivisatos, *Nat. Biotechnol.*, 2005, **23**, 741–745.

48 Y. Mei, G. Sharma, Y. Lu and M. Ballauff, *Langmuir*, 2005, **21**, 12229–12234.

49 M. A. Bhosale, D. R. Chenna, J. P. Ahire and B. M. Bhanage, *RSC Adv.*, 2015, **5**, 52817–52823.

50 M. Guo, J. He, Y. Li, S. Ma and X. Sun, *J. Hazard. Mater.*, 2016, **310**, 89–97.